

1 **Insights of warm cloud biases in CAM5 and CAM6 from the single-column modeling**
2 **framework and ACE-ENA observations**

3 **Yuan Wang^{1,4,*}, Xiaojian Zheng², Xiquan Dong², Baike Xi², and Yuk L. Yung³**

4 ¹Department of Earth, Atmosphere, and Planetary Sciences, Purdue University, West Lafayette,
5 IN, USA

6 ²Department of Hydrology and Atmospheric Sciences, University of Arizona, Tucson, AZ, USA

7 ³Division of Geological and Planetary Sciences, California Institute of Technology, Pasadena,
8 CA, USA

9 ⁴Now at Department of Earth System Science, Stanford University, Stanford, CA, USA

10
11 *Corresponding author: Yuan Wang (yzwang@stanford.edu) Deleted: yuanwang@purdue.edu

13 **Abstract**

14 There has been a growing concern that most climate models predict too frequent precipitation,
15 likely due to lack of reliable sub-grid variability and vertical variations of microphysical processes
16 in low-level warm clouds. In this study, the warm cloud physics parameterizations in the single-
17 column configurations of NCAR Community Atmospheric Model version 6 and 5 (SCAM6 and
18 SCAM5, respectively) are evaluated using ground-based and airborne observations from the DOE
19 ARM Aerosol and Cloud Experiments in the Eastern North Atlantic (ACE-ENA) field campaign
20 near the Azores islands during 2017-2018. Eight-month SCM simulations show that both SCAM6
21 and SCAM5 can generally reproduce marine boundary-layer cloud structure, major macrophysical
22 properties, and their transition. The improvement of warm cloud properties from CAM5 to CAM6
23 physics can be found compared to the observations. Meanwhile, both physical schemes
24 underestimate cloud liquid water content, cloud droplet size, and rain liquid water content, but
25 overestimate surface rainfall. Modeled cloud condensation nuclei (CCN) concentrations are
26 comparable with aircraft observed ones in the summer but overestimated by a factor of two in
27 winter, largely due to the biases in the long-range transport of anthropogenic aerosols like sulfate.
28 We also test the newly recalibrated autoconversion and accretion parameterizations that account
29 for vertical variations of droplet size. Compared to the observations, more significant improvement
30 is found in SCAM5 than in SCAM6. This result is likely explained by the introduction of sub-grid
31 variations of cloud properties in CAM6 cloud microphysics, which further suppresses the scheme
32 sensitivity to individual warm rain microphysical parameters. The predicted cloud susceptibilities
33 to CCN perturbations in CAM6 are within a reasonable range, indicating significant progress since
34 CAM5 which produces too strong aerosol indirect effect. The present study emphasizes the
35 importance of understanding biases in cloud physics parameterizations by combining SCM with
36 in situ observations.

1. Motivation and Background

Marine boundary-layer (MBL) clouds are crucial for the global radiation budget, as they efficiently regulate the solar radiation reaching the ocean surface (Dong et al., 2022) and largely determine the climate sensitivity (Sherwood et al., 2020). However, numerical simulations of MBL clouds in global climate models (GCM) remain challenging, mainly due to the mismatch of the spatial scales of MBL clouds (tens of meters) and GCM grids (~ 100 km). Therefore, empirical parameterizations of subscale cloud properties and variabilities, for both microphysics and macrophysics, play a critical role in predicting MBL clouds and precipitation in GCM (Wang et al., 2013). Consequently, how to constrain and improve those cloud parameterizations using the state-of-the-art observations become an important issue. One challenging aspect of the GCM cloud evaluation lies in the tight coupling between cloud physics and dynamics, as cloud microphysics can feedback to dynamics and thermodynamics through heating profile alteration or radiation flux interference (Wang et al., 2014, 2020).

To better probe the uncertainty source in the cloud physical parameterizations, a simplified GCM configuration has been developed to separate cloud physics from large-scale dynamical and thermodynamical conditions. The so-called single column model (SCM) is ideal for utilizing in situ observations from the field campaigns that are normally conducted intensively over the targeted area (Zhao et al., 2021). The modeling framework adopted in this study, NCAR Community Earth System Model (CESM), has a long history of providing such a modeling tool along with the development of its comprehensive models (Liu et al., 2007; Gettleman et al., 2019). With more added features and enhanced representations of cloud and aerosol in the cloud physical parametrizations in CESM version 1 and 2, it is valuable to evaluate the single-column versions of them using the recent field measurements.

The Eastern North Atlantic (ENA) is an ideal place around the world to study MBL clouds, considering the prevailing MBL cloud occurrence, diverse mesoscale meteorological conditions (Jensen et al., 2021; Zheng et al., 2022a), and distinctive aerosol sources (Wang, J. et al., 2021). A recent field campaign, the Aerosol and Cloud Experiments in the Eastern North Atlantic (ACE-ENA) provide ample ground-based and in situ aircraft observations of cloud micro- and macrophysics, aerosol properties, as well as atmospheric states over a whole summer and winter (Wang, J. et al. 2021; Wu et al., 2020). Recent WRF large-eddy simulations (LES) driven by the ERA5 reanalysis over the ENA well reproduce the general vertical variations of meteorological

Deleted: Dong et al., 2022;

69 factors and cloud cellular structure (Wang et al., 2020). Meanwhile, LES and observations exhibit
70 substantial discrepancies in the evolution of MBL clouds in two selected stratocumulus cases
71 during the ACE-ENA field campaign, likely due to the biases in both warm cloud physical
72 parameterizations and meteorological conditions as external forcing. Those issues motivate us to
73 look for stronger observational constraints in the single-column framework which minimizes the
74 propagated errors from large-scale forcing. In this study, we use the ARM 3-hourly large-scale
75 forcing of atmospheric states specifically developed for the ACE-ENA Intensive Observation
76 Periods (IOP) to drive SCM.

77 The uncertainties of warm cloud physics in the atmospheric component of CESM1/2 have
78 been reported in many previous studies (e.g. Kay et al., 2016; Zhao et al., 2022), while most of
79 them focused on addressing the issues on the global scale. Leveraging the continuous radar
80 retrievals of MBL cloud and drizzle microphysical properties during ACE ENA, Dong et al. (2021)
81 modified the parameterizations of two key processes in warm cloud microphysics in CAM5, i.e.,
82 autoconversion from cloud droplets to rain drops and accretion of cloud droplets by raindrops.
83 They showed that by applying this set of new parameterizations to CAM5 in global climate
84 simulations, precipitation frequency is generally reduced but with enhanced intensity mainly in the
85 mid-latitude regions, alleviating the long-lasting issue in the climate models, e.g., “too frequent
86 and too light precipitation”. Even the cloud radiative effect and top-of-atmosphere radiative flux
87 simulations can be improved consequently. Meanwhile, a remaining question lies in whether such
88 a new scheme works well over the location where the radar observational constraints come from
89 originally. The single-column modeling framework enables us to examine the effect of the
90 modified microphysical scheme on the local scale.

91 2. Methodology

92 2.1 Single column version of Community Atmospheric Model

93 In this study, we use single-column configuration of Community Atmospheric Model
94 version 6 (referred to as SCAM6 thereafter) in the Community Earth System Model (CEMS 2.1.1).
95 NCAR CESM is a community GCM that has been widely used to study the climate change (e.g.
96 Yeager et al., 2018), precipitation extremes (e.g. Wang et al., 2016), cloud processes (e.g. Kay et
97 al., 2012), and aerosol-cloud-radiation-circulation feedbacks in the Earth system (e.g. Wang et al.,
98 2015). The atmosphere component of CESM2 (CAM6) has been modified substantially with a
99 range of enhancements and improvements for the representation of physical processes since its last

Deleted: large-scale

Deleted: Therefore

Deleted: and outstanding

Deleted: Wang

Deleted: 2018

version, CAM5. In particular, the modifications on the aerosol and cloud parameterizations are extensive. For example, a multivariate PDF-based third-order turbulence closure parameterization scheme, Cloud Layers Unified By Binormals (CLUBB), is implemented to unify the representation of boundary layer, shallow convection, and stratiform macrophysics in the model (Bogenschutz et al., 2013; Golaz and Larson, 2002). The two-moment cloud microphysical scheme is updated to version 2 (MG2, Gettelman and Morrison, 2015) with warm rain parameterization remaining as the Khairoutdinov & Kogan (2000) scheme (hereafter called KK). Major updates on cloud microphysics include prognostic precipitation (rain and snow), sub-stepping technique, and re-tuned autoconversion scheme which is critical for aerosol indirect effect on cloud lifetime and precipitation (Malavelle et al., 2017). The strong coupling between CLUBB and MG2 also enables interactions between subgrid shallow cloud, aerosol, and environment. Deep convection remains parameterized by the Zhang-McFarlane (1995) scheme and has been re-tuned to increase the sensitivity to convective inhibition. Parameterizations of homogeneous ice nucleation and heterogeneous immersion nucleation in cirrus clouds (Liu and Penner, 2005) explicitly consider the effects of sulfate and dust aerosol serving as ice nuclei on the cold clouds.

The Modal Aerosol Module (MAM) in CESM is updated from a three-mode to four-mode approach (MAM4) to better consider the aging processes of black carbon in the atmosphere (Liu et al., 2016; Wang et al., 2018). Six types of aerosols with different hygroscopicity and optical properties are considered in MAM3, including sulfate, black carbon (BC), primary organic matter (POM), secondary organic aerosol (SOA), dust and sea salt. The aerosol module accounts for most of the important processes associated with atmospheric aerosols, including emission, nucleation, coagulation, condensational growth, gas and aqueous-phase chemistry, dry deposition, in-cloud and below-cloud scavenging, re-production from evaporated cloud droplets and suppression, as well as agricultural, deforestation, and peat fires (Li and Lawrence, 2017). To test the impacts of cloud physical parameterization on the model fidelity, we also conduct the single-column simulations using the CAM5 physics (SCAM5) under the same large-scale forcing data.

Because the ACE-ENA is a relatively new field campaign and does not have a pre-defined case in SCAM6, we create a new case in CAM6 based on a new set of large-scale data for this IOP. The large-scale forcing over the ARM-ENA is developed from the constrained variational analysis (VARANAL, Xie et al., 2004; Tang et al., 2019). It includes air temperature (T) and moisture (q), their horizontal and vertical advection, surface sensible and latent heat fluxes, U and

Deleted: its

Deleted: by incorporating

Deleted: facilitates

Deleted: -

Deleted: -

Deleted: interactions

Deleted: , which could potentially signify the impact of absorbing aerosols within the planetary boundary layer (PBL)....

Deleted: aerosol module

Deleted: To cover the full IOP in our simulations, we run SCAM over 8 months from June 1, 2017, to Feb 1, 2018.

V winds, large-scale vertical motion/velocity, TOA/surface radiation fluxes, etc. VARANAL is based on ERA5 reanalysis (Copernicus Climate Change Service, 2017) with the additional input of observations from the ARM ENA site incorporated into the variational analysis, to represent the atmospheric states over a Global Climate Model (GCM) grid box. The original VARANAL data is produced specifically for the ACE-ENA IOP, with a temporal resolution of 3-hour and 45 vertical levels.

To minimize the biases in aerosol advection and dynamical forcing, aerosol and the temperature fields are nudged to their initial conditions on different timescales, varying from 10 days at the bottom of the model to 2 days at the top of the model (Gettelman et al., 2019). Also, to simulate the right seasonal variations of aerosol and temperature initial conditions, each of our model integration only lasts one month, and a new sequential run will follow with updated initial conditions. By doing so the seasonality of aerosols will follow that of climatology on the monthly basis. CAM6 model has 32 vertical levels from the surface to 2 hPa (about 45 km), while CAM5 have 30 levels. The two models both use a time step of about 30 minutes, while CAM6 uses sub-stepping for microphysical processes.

2.2 Numerical experiment design

To cover the full IOP in our simulations, we run SCAM5 and SCAM6 over 8 months from June 1, 2017, to Feb 1, 2018, as control experiments (Ctrl). To explore the possible sources of biases in simulated drizzle and LWC, we employ a retuned KK scheme (Dong et al., 2021, thereafter as D21-KK) that explicitly links the autoconversion and accretion rates with mass mean cloud droplet radius ($r_{m,c}$). The original KK scheme is expressed as below:

$$R_{auto}(Z) = \left(\frac{\partial q_r}{\partial t} \right)_{auto} = A q_c^{a1}(Z) N_c^{a2}, \quad (1)$$

and,

$$R_{accr}(Z) = \left(\frac{\partial q_r}{\partial t} \right)_{accr} = B (q_c(Z) q_r(Z))^b, \quad (2)$$

where $A = 1350$, $a1 = 2.47$, and $a2 = -1.79$ in CAM5. In D21-KK, both autoconversion and accretion rates are further aware of the vertical variations of r_c , so the constant A and B are replaced as a function of r_c :

$$R'_{auto}(Z) = \frac{RLWC(Z)}{\int \rho_{air} P_r(Z) dt} R_{auto}(Z) = A'(Z) q_c^{2.47}(Z) N_c^{-1.79}, \quad (3)$$

and,

Deleted: 2.2

Moved (insertion) [1]

Moved (insertion) [2]

Moved (insertion) [3]

$$R'_{accr}(Z) = \frac{RLWC(Z)}{\int \rho_{air} P_r(Z) dt} R_{accr}(Z) = B'(Z) (q_c(Z) q_r(Z))^{1.15}, \quad (4)$$

where A' and B' are further parameterized in CAM5 as:

$$A'(Z) = 121683 \times \exp(-0.528 r_{m,c}(Z)) + 364, \quad (5)$$

and,

$$B'(Z) = 632 \times \exp\left(-24.5 \frac{r_{m,c}(Z)}{r_{m,r}(Z)}\right) + 51, \quad (6)$$

CAM6 microphysics aims to reduce the autoconversion dependency on the N_c , so α_2 and A are set as -1.1 and 13.5, respectively, with α_2 unchanged. We did the same recalibration for CAM6 autoconversion processes, and the corresponding A' is parameterized as:

$$A'(Z) = 3359 \times \exp(-0.721 r_{m,c}(Z)) + 8, \quad (7)$$

Hence the updated autoconversion for CAM6 microphysics has the form as below:

$$R'_{auto}(Z) = \frac{RLWC(Z)}{\int \rho_{air} P_r(Z) dt} R_{auto}(Z) = f_e A'(Z) q_c^{2.47}(Z) N_c^{-1.1}, \quad (8)$$

Where f_e represents an enhancement factor which is diagnosed from the CLUBB to account for sub-grid variabilities of cloud and rain.

In another set of sensitivity experiment, to explore the aerosol indirect effect on cloud and warm precipitation, we scale up aerosol number and mass concentrations in the accumulation mode by a factor of 2 in the initial condition. Such an experiment is named as “pAero”. Moreover, to examine the sensitivity of cloud simulations to the large forcing data, we perturb specific humidity state variable and related tendency terms, with an experiment name “ForcingQ Adj”. All the above experiment are summarized in Table 2.

2.3 ACE-ENA observations

Aircraft in situ observations during the ACE-ENA provide best available characterizations of cloud and aerosol vertical distributions, with differentiation of aerosol types and hygroscopicity. During the two IOPs, 39 flights were deployed to collect data for 39 days, 20 in the summer IOP, 19 in the winter IOP. Meanwhile, ground-based observations were conducted simultaneously and consecutively. Based on the Ka-band ARM Zenith Radar (KAZR) measurements, cloud and rain microphysical properties (cloud droplet effective radius, r_c ; cloud droplet number concentration, N_c ; cloud liquid water content, $CLWC$; rain droplet mass median radius, $r_{m,r}$; rain droplet number concentration, N_r ; and rain liquid water content, $RLWC$) over the ARM ENA site can be retrieved

Moved (insertion) [4]

Moved (insertion) [5]

Moved (insertion) [6]

(Wu et al. 2020). The cloud and drizzle microphysical retrievals were validated by the aircraft in situ measurements from ACE-ENA field campaign, with the estimated median uncertainties of $\sim 15\%$ for $r_{c,s}$, $\sim 30\%$ for $r_{m,r}$, $\sim 30\%$ for N_c and $CLWC_s$, and $\sim 50\%$ for N_r and $RLWC$. Note that the subscript “c” denotes cloud and subscript “r” denotes rain. The model counterparts are extracted and compared with the retrieval, except the $r_{m,r}$ which is not an output from the model. Following the method in Wu et al. (2020) equation 2a, the $r_{m,r}$ can be calculated by:

$$r_{m,r} = \left(\frac{RLWC * 3.67^4}{\rho_w * N_w * 8\pi} \right)^{1/4} \quad (9).$$

where the ρ_w is water density, and the N_w is the normalized drizzle number concentration ($N_w = N_r / r_{m,r}$). Furthermore, the $CLWC$ ($RLWC$) is scaled by the cloud (rain) fraction within the grid box to match the retrievals.

For the aircraft in situ measurements of aerosol, the Passive Cavity Aerosol Spectrometer (PCASP) measured the aerosols with the size range from $0.1 \mu m$ to $3.2 \mu m$ (Goldberger, 2020), hence the accumulation-mode aerosol number concentration (N_{Acc}) can be derived from the PCASP $0.1 \mu m$ to $1.0 \mu m$ measurement. The CCN number concentration (N_{CCN}) is obtained by the CCN-200 particle counter on board the G-1 aircraft. The N_{CCN} is a measurement under the controlled supersaturation of 0.35% with a humidified particle size range from 0.75 to $10 \mu m$ (Uin and Mei, 2019). The PM1 aerosol chemical components mass concentrations are measured by the Aerodyne High-Resolution Time-of-Flight Aerosol Mass Spectrometer (HR-ToF-AMS). The accuracy of each individual instrument can be found in the instrument handbooks available on the ARM website.

We select only those research flights that followed a horizontal track within one grid size of the CAM models (1.25° longitude and 0.9° latitude), centered on the ARM-ENA site. Also, to meet the criteria for comparison with SCAM, each aircraft case must include comprehensive vertical sampling of cloud and aerosol within the specified time period. To ensure the apple-to-apple comparison between model and observations, the cloud and rain samples are selected following the same criteria: 1) $4 \mu m < r_c < 25 \mu m$; 2) $CLWC > 0.01 gm^{-3}$; 3) $N_c > 1 cm^{-3}$; and 4) $RLWC > 1 \times 10^{-4} gm^{-3}$. The geopotential height from the model output is extracted for each time step, hence the quantities at pressure level can be converted to height level and compared with the observation results. Both model and observation results are limited to below 3km.

3. Evaluation of SCAM using ACE-ENA observations

Deleted: -

Deleted: 1),

Deleted: and

Deleted: are

Deleted: -

Deleted:

Deleted: To make better comparisons, this study

Deleted: selects the

Deleted: with

Deleted: 'L' shape pattern center at

Deleted: -

Deleted: The SCAM6 samples are selected within

Deleted: time duration of the

Deleted: cases. Note that the aircraft cases are selected up to end of Jan 2018 due to the end of SCAM6 simulations

Deleted: SCAM6

252 3.1 Meteorological conditions

253 To understand the cloud and drizzle property differences between simulations and
254 observations, we first evaluate the SCAM6 simulated meteorological conditions by the ARM
255 Interpolated Sonde (INTERPSONDE) value-added product (VAP), which is an independent
256 dataset from the large-scale forcing data used to drive SCM. As shown in Fig. 1a, the simulated
257 air temperature (T_{air}) values are generally comparable to the observed ones with clear seasonal
258 variations. The statistics from the 8-month simulations shows that the differences in both mean
259 and median T_{air} agree within 1% to the observed ones (Fig. 1c). However, the probability
260 distribution functions (PDF) reveal some cancelling effect behind the good agreement on the
261 means: the simulated values over the temperature “extremes” (lower and higher bins) are larger
262 than the observed ones, but in the middle bins, the observed values surpass the simulated ones (for
263 the bins between 280 and 290 K). Essentially, the modeled T_{air} PDF is wider than the observed
264 one. The discrepancy of the moisture field is more evident. Even though the model captures the
265 evolution of relative humidity (RH) throughout 8 months, both mean and median RH have ~10%
266 bias in the model. In particular, the biases become severe when RH values fall into the high
267 humidity regime. The RH frequency within the 90-100% range is about two times higher in
268 SCAM6 than the observations. A comparison of specific humidity (SH) shows that SCAM6
269 overpredicts SH by 11.8%, indicating that the RH bias stems mainly from the absolute moisture
270 bias. The similar statistics for the grids with RH larger than 90% shows the discrepancy in SH is
271 still larger than that of T_{air} (Fig. S1), indicating larger contribution of SH to RH biases than T_{air} . It
272 can be explained by the fact that temperature field is relaxed to the input as an additional constraint,
273 while SH is predicted as a fully prognostic variable in SCM. We will examine the potential impact
274 of moisture uncertainty in the large-scale forcing data on the cloud property simulation through
275 sensitivity, and the results will be discussed below.

276 3.2 Cloud properties

277 We first compare CLWC and RLWC over time and altitude dimensions between SCAM6
278 simulations and ARM radar-lidar-MWR retrievals (Figure 2a-d). The simulated CLWC values in
279 both time and altitude are generally consistent with the ARM retrievals. More specifically, SCAM6
280 can capture those vertically thick clouds in early November and middle December due to the
281 prevalent frontal systems during that time of the year. However, some high CLWC values are not
282 reproduced in the model. Similarly, the temporal evolution of simulated RLWC agrees with the

Deleted: the

Deleted: I

Deleted: , supporting the high fidelity of the model to reproduce the temperature field. The situation of the moisture field is slightly different.

Deleted: more

Deleted: Observation.

Deleted: , instead

Deleted: temperature bias

292 retrievals as demonstrated in Figure 2c-d, however, their magnitudes are much lower than the
 293 retrievals. The relatively coarse vertical resolution near the planetary boundary layer (PBL) is
 294 discernable from the discretized cloud vertical distribution in the model simulations (Fig. 2a, c).
 295 However, the vertical development of different cloud types (stratus, stratocumulus, and cumulus)
 296 and their transitions are generally reproduced by SCAM6. When cumulus occurs with cloud top
 297 height greater than 2000 m, the model can always capture them. Despite good agreement on cloud
 298 top height, SCAM6 overpredicts CLWC and RLWC frequency near the surface (< 200 m)
 299 compared to the observations. The statistics of cloud macrophysics in Fig. 3 supports the analyses
 300 above. Cloud top heights show good agreement between SCAM6 and observations, with 8-month
 301 mean values of 1561 m and 1425 m, respectively (Fig. 3f). It corroborates the notion that SCAM6
 302 can capture the cloud type transition relatively well. However, due to the lower cloud-base height
 303 in SCAM6, cloud physical thickness is overestimated in the model. Even with the above biases in
 304 cloud macrophysics, the modeled cloud mass center (CMC) height (mean cloud layer heights
 305 weighted by CLWC) is comparable to the observed ones (Fig. 3h).

306 A further comparison of 8-month surface precipitation rate in Fig. 2e and 2f shows that
 307 SCAM6 can capture the heavy precipitation (>25 mm/day) under the large-scale forcing during
 308 the winter season (Oct. to Jan.). However, the “too-frequent-drizzle” issue persists throughout the
 309 8-month simulations. The frequency of light precipitation (< 2 mm/day) is more than 80% which
 310 is rather unrealistic compared to the observations. The mean surface precipitation in SCAM6 is
 311 overestimated by 30% compared to the rain gauge measurements during the whole 8-month period.

312 The statistical comparisons of cloud and drizzle microphysical properties in Fig. 3a-d
 313 reveal that CLWC is overestimated by about 30%. Consequently, r_c is slightly larger in the model,
 314 and the bias becomes worse for those larger droplets (r_c greater than 10 micron). Too large CLWC
 315 fosters fast cloud to warm rain conversion, but the simulated RLWC values are smaller than the
 316 retrievals, leading to too frequent surface precipitation mainly in the drizzle form. Note that
 317 retrieved RLWC from ground-based radar also bears with large uncertainty, as indicated by the
 318 large error bar in Fig. 3c. Hence the real differences of RLWC between SCAM6 and observations
 319 remain hard to be quantified. Our analyses here include all 8-month simulation results and all types
 320 of cloud. In an additional analysis, by focusing on the marine boundary layer (MBL) stratiform
 321 cloud only, we obtain quite similar cloud evaluation results. As shown in Fig. S2, then we
 322 strengthen our selection criteria by only sampling consecutive cloud layers lasting more than 2

Deleted: PBL

Deleted: clout

Deleted: -

Deleted: simulation

Deleted: Observation

Deleted: one

Deleted: Observation

Deleted: during this time.

Deleted: we focus

Deleted: but get

Deleted: S1

hours with the cloud top height less than 3 km, the statistics of cloud micro- and macro- physical properties do not differ significantly. It reflects the fact that over the ENA, MBL clouds are predominated during those seasons. In observation of the SH bias against observations (Fig. 1), additional SCAM6 sensitivity test is conducted by perturbing moisture content and the associated advection with a scaling factor of 0.85. Results show that the distributions of simulated SH and RH only slightly shift towards the lower tail with smaller mean values, which cannot correct their biases. Notably, despite the minor changes in the simulated cloud and drizzle microphysics, the cloud top height, thickness, and CMC simulations perform noticeably better than the control simulation (Fig. S3). It suggests that the moisture fields in the large-scale forcing exert larger impacts on the simulated cloud structure and macrophysics than the microphysics. In other words, cloud microphysical properties are strongly regulated by the parameterizations in the model, and less sensitive to the external forcing.

Driven by the same large-scale forcing, SCAM5 simulated meteorological fields are similar to SCAM6 (Fig. S4), but cloud properties are quite different from those by SCAM6. Instead of an overestimation in SCAM6, the SCAM5 simulated CLWC exhibits an underestimation (Fig. 4a). One possible reason is the change of formula for the saturation vapor pressure in the MG2 cloud microphysics scheme (Gettelman and Morrison, 2015). Previous SCM simulations for the MPACE case also show the larger LWC by MG2 than MG1 (Gettelman et al., 2015). The good agreement of the mean r_c in SCAM6 does not exist in the SCAM5 simulations (Fig. 4b), and too many small cloud droplets (less than 6 micron) are present in SCAM5, which are not found in either observation or SCAM6. RLWC in SCAM5 is still much smaller than observations (Fig. 4c), suffering the similar issue to SCAM6. Different from SCAM6, SCAM5 overpredicts mean $r_{m,r}$ (Fig. 4d) but underpredicts mean r_c . The high bias in drizzle size is likely related to the too strong raindrop accretion process, while the low bias in drizzle amount is subject to both source and sink uncertainty with the drizzle budget. The mean surface precipitation in SCAM5 is 0.082 mm/day (Fig. S5), higher than the 0.056 mm/day in observation and 0.073 in SCAM6. The anomalously high surface precipitation lines up with too large drizzle size and too low drizzle amount suspended in the air in SCAM5.

The improvement of the cloud macrophysics from SCAM5 to SCAM6 is more evident than that of microphysics. Too low cloud-base height and cloud-top height result in too thin cloud deck in SCAM5 (Fig. 4e-g). The cloud center mass is also systematically low in SCAM5. By and large,

Deleted: heights

Deleted: specific humidity

Deleted: the

Deleted: -

Deleted: and

Deleted: the

Deleted: S2

Deleted: .

Deleted: single-column

Deleted: ,

Deleted: Observation,

Deleted: Differing

Deleted: underpredict

Deleted: but

Deleted: indicate that the sources of those biases can be different

Deleted: the model.

Deleted: .

Deleted: Overall speaking

384 the updated cloud physics in CAM6 ~~helps~~ improve many aspects of cloud simulations, but the
 385 drizzle issues still linger on.

Deleted: help

386 3.3 Aerosols

387 To probe the possible uncertainty sources for cloud droplet number concentration, vertical
 388 profiles of aerosol and CCN number concentrations are compared between SCAM6 simulations
 389 and ~~in situ~~ aircraft observations from 17 flights ~~near the Azores islands~~ during the ACE-ENA field
 390 campaign (Fig. ~~5~~). ~~The in situ profiles represent the average of data collected during 12 flights and~~
 391 ~~5 flights selected during the summer and winter IOPs, respectively. The SCAM6 profiles~~
 392 ~~correspond to the averages within the 17-flight time-stamps.~~ SCAM6 generally gets seasonality
 393 right, i.e., aerosol and CCN number concentrations are high in summer and low in winter. The
 394 model also agrees with observations on the magnitude of accumulation-mode aerosol
 395 concentration (N_{ACC}) and CCN concentration (N_{CCN}) during the summer, which further leads to a
 396 reasonable comparison of N_C . The small bias of N_C generally follows the performance of N_{CCN} ,
 397 i.e., high bias near the bottom while low bias near the top. One intriguing phenomenon during
 398 the summertime is that N_{CCN} can be even higher than N_{ACC} , found in both aircraft measurements
 399 and model simulations. The high N_{CCN} occurs within the MBL (<1000 m) in SCAM6. In contrast,
 400 measured N_{CCN} in lower free troposphere (FT, 2000-2500 m) is of the same magnitude with that
 401 within MBL, and FT N_{CCN} is higher than N_{ACC} in the observations. A breakdown of aerosol number
 402 concentration budget in SCAM6 (Fig. ~~S6~~) shows that Aitken-~~mode~~ aerosols contribute to about
 403 20% summertime and 45% wintertime total aerosol numbers. In contrast, the coarse-~~mode~~ aerosol
 404 number is only about 1% of the Aitken-~~mode~~ one. Therefore, the large N_{CCN} within the MBL in
 405 SCAM6 should be attributed to the efficient Aitken-~~mode~~ aerosol activation near the cloud bottom
 406 in SCAM6. A further examination of aerosol chemical ~~compositions~~ in SCAM6 suggests that
 407 sulfate is the predominated aerosol species in the Aitken ~~mode~~ (Fig. ~~S7~~).

Deleted: in situ

Deleted: 5).

Deleted: S3

Deleted: model

Deleted: model

Deleted:

Deleted: model

Deleted: composition

Deleted: model

Deleted: S4).

Deleted: observational data

Deleted: somewhat

408 Understanding larger N_{CCN} than N_{ACC} in the lower FT in the ~~observations~~ is challenging,
 409 because coarse- and Aitken- mode aerosol number concentrations was not measured during the
 410 IOP. However, previous study found that new particle formation frequently occurs in the FT over
 411 the ENA, because of the sulfuric acids being elevated, especially during summertime where the
 412 oceanic dimethyl sulfide (DMS) emissions are strong (Zawadowicz et al., 2021). Previous back-
 413 trajectory analyses by Wang et al. (2020) suggest the long-range transport of the fine-mode
 414 aerosols to the ENA site likely originates from the continental U.S. Therefore, the oxidations of

428 DMS, jointly with the long-range transported pollution, contribute to the elevated Aitken-mode
 429 aerosol concentrations in the FT. Those Aitken-mode aerosols (e.g., DMS oxides and diluted
 430 continental pollutants) are found to be substantial contributors to the CCN budget (Wang et al.,
 431 2021). The FT aerosols and CCN can be further entrained down to the MBL, consistent with what
 432 is shown in Fig. 5. Note that SCAM6 predicts the “top-heavy” Aitken model aerosol concentration
 433 profile, but it does not lead to the larger N_{CCN} above the MBL. Hence, we can only speculate that
 434 in the real atmosphere, there are significant Aitken mode aerosols that can serve as CCN in the
 435 lower FT, but that is not the case in SCAM6. The above discussions reinforce the notion that it is
 436 crucial to accurately simulate the long-range transport of aerosols and their growth over a remote
 437 maritime region like ENA. And future investigation on how the aerosol activation process is
 438 simulated in different model levels is warranted.

439 During the winter, N_{ACC} is comparable between model and observation (Fig. 5d), while
 440 N_{CCN} is significantly overestimated from the surface to 2000 m altitude (Fig. 5e). Based on our
 441 analyses above for the summer, we can infer that too strong contribution from the Aitken mode to
 442 the CCN budget also exists in winter. Moreover, there is a non-negligible effect that the frequent
 443 convective activities and associate large super saturation within the mid-latitude frontal systems
 444 during wintertime also likely result in the stronger activation of Aitken mode aerosol. Surprisingly,
 445 the modeled N_c shows good agreement with observations, despite the overestimated N_{CCN} . One
 446 plausible reason is the canceling effect from the too strong N_c sink in the model. The
 447 overestimated cloud droplet size by the model (Fig. 3b) fosters the warm rain formation, and in
 448 turn, efficiently deplete cloud droplets (Zheng et al., 2022b), keeping the modeled N_c at a
 449 comparable level with the observations.

450 4. Impacts of new observation-constrained warm rain parameterizations

451 Our previous study showed that this set of new parameterizations in CAM5 help alleviate
 452 the long-lasting issue in the climate models, e.g., “too frequent and too light precipitation”, on the
 453 global scale (Dong et al., 2021). When we apply the same set of parameterizations in SCAM5 over
 454 the ENA (referred to as SCAM5_{D21}), we find similar improvements on cloud and precipitation
 455 properties. As shown in Fig. 6, CLWC in SCAM5_{D21} is elevated due to the less efficient
 456 autoconversion scheme, and the simulated CLWC values agree better with the ARM retrievals
 457 compared with original SCAM5. r_c is also enlarged in SCAM5_{D21}, being more consistent with
 458 retrievals. The mass median radius of raindrops $r_{m,r}$ are reduced slightly, while there is no

Deleted: processes are being

Deleted: ,

Deleted: .

Deleted: overestimated

Deleted: it

Deleted: stronger

Deleted: due to

Deleted: frequent

Deleted: passages

Deleted: In contrast

Deleted: surprisingly

Deleted: in

Deleted:). Larger cloud droplets facilitate the autoconversion and accretion processes

Deleted: observed

Deleted: model simulation

Moved up [1]: To explore the possible sources of biases in simulated drizzle and LWC, we employ a retuned KK scheme (Dong et al., 2021, thereafter as D21-KK) that explicitly links the autoconversion and accretion rates with mass mean cloud droplet radius ($r_{m,c}$).

Moved up [2]: $R_{auto}(Z) = \left(\frac{\partial q_r}{\partial t}\right)_{auto} = A q_c^{a1}(Z) N_c^{a2}$,

(1) and,

$R_{accr}(Z) = \left(\frac{\partial q_r}{\partial t}\right)_{accr} = B (q_c(Z) q_r(Z))^b$,

(2)

where $A = 1350$, $a1 = 2.47$, and $a2 = -1.79$ in CAM5.

Moved up [6]: aims to reduce the autoconversion dependency on the N_c , so $a2$ and A are set as -1.1 and 13.5, respectively, with $a2$ unchanged.

Moved up [3]: In D21-KK, both autoconversion and accretion rates are further aware of the vertical variations of r_c , so the constant A and B are replaced as a function of r_c :
 $R'_{auto}(Z) = \frac{RLWC(Z)}{\int \rho_{air} P_r(Z) dt} R_{auto}(Z) = A'(Z) q_c^{2.47}(Z) N_c^{-1.79}$,
 (3)

Moved up [4]: $(-0.528 r_{m,c}(Z)) + 364$,

Moved up [5]: $(-24.5 \frac{r_{m,c}(Z)}{r_{m,r}(Z)}) + 51$

Deleted: The original KK2000 scheme is expressed as ... [1]

Deleted: CAM6

Deleted: 121683exp

Deleted: (5)

Deleted: .

Deleted: .

Deleted: becoming

522 significant change in RLWC in SCAM5_{D21}. Because of the improved cloud microphysical
 523 properties, cloud macrophysics also match up better with observations. Cloud base height, cloud
 524 top height, and cloud mass center height are all improved to some extent in SCAM5_{D21} simulations,
 525 (Fig. 6e-h). These comparisons are encouraging, indicating that the D21-KK new warm
 526 parameterizations in SCAM5 make significant improvements on the simulated MBL cloud and
 527 drizzle properties.

528 Different from the CAM5 microphysics, CAM6 starts to introduce sub-grid cloud
 529 variations (Lebsock et al., 2013; Zhang et al., 2020) and re-tuned the parameters in the KK2000
 530 scheme. One direct consequence is that CLWC has been changed from underestimation to
 531 overestimation (Fig. 7a). Therefore, an even slower autoconversion process with the new D21-KK
 532 scheme cannot further benefit the warm rain processes in CAM6. As expected, SCAM6_{D21} does
 533 not exhibit improvement in simulating both cloud microphysics and macrophysics (Fig. 7).
 534 Distinctive sensitivities to the same microphysical parameter modification under different versions
 535 of the physics package poses a challenge on model improvement through only updating a certain
 536 set of parameterizations.

537 5. Assessing aerosol indirect effects under the single-column frameworks

538 Aerosol indirect effects, especially the second indirect effect concerning the liquid water
 539 content change, was reported to be over-predicted in CAM5 when simulating the aerosol
 540 perturbations, such as volcano eruptions, on the low clouds (Malavelle et al., 2017). Here we assess
 541 the aerosol first and second indirect effects of CAM6 over the ENA under the single-column
 542 framework. To perturb the CCN budget, we choose to modify the accumulation-mode aerosols in
 543 their initial conditions. As the aerosol relaxation is on, such a perturbation is expected to constantly
 544 impact the aerosol field during the integrations. Considering the relatively low background aerosol
 545 concentration over ENA, the change in aerosol direct effect on the clear-sky radiation fluxes can
 546 be ignored in this setup. Both aerosol number and mass concentrations in the accumulation mode
 547 are enlarged by a factor of 2, the results are labeled as S6_{pAero} and are compared with the original
 548 SCAM6 simulations (Fig. 8). With such an aerosol perturbation, N_{CCN} within MBL (< 1km) is
 549 increased from 112.5 to 175.8 cm⁻³, corresponding to a 56% enhancement. Similarly, CCN in the
 550 lower FT and upper MBL (1-3 km) increased by 61%. Aerosol first and second indirect effects are
 551 evident in SCAM6, as reduced τ_c and increased CLWC are both found in the perturbed experiment.
 552 We further quantify the droplet size susceptibility and cloud water susceptibility with respect to

Deleted: (Fig. 6e-h)

Deleted: .

Deleted: cloud LWC

Deleted: packages

Deleted: path

Deleted: LWC

559 MBL CCN changes by $\frac{\partial \ln(r_c)}{\partial \ln(N_{CCN})}$ and $\frac{\partial \ln(CLWC)}{\partial \ln(N_{CCN})}$, respectively. The SCAM6 simulated droplet size
 560 susceptibility is -0.2 , close to the LES simulated range from -0.22 to -0.25 and the upper bound
 561 of the observed range over ENA (Wang et al., 2020; Zheng et al., 2022a). The SCAM6 simulated
 562 cloud water susceptibility is $+0.19$ which also falls into the LES prediction ($+0.18$ to $+0.30$). Those
 563 results suggest that the newly introduced sub-grid cloud variabilities in SCAM6 can account for
 564 the aerosol indirect effects at a reasonable level. Mean surface precipitation amount shows
 565 ~~relatively~~ small responses to CCN perturbation (less than 2%), because convective precipitation in
 566 early winter dominates the study period while deep convective parameterization in SCAM6 is still
 567 unlinked with cloud microphysics and unaware of CCN effects so far. Cloud top height (Z_T) shows
 568 an increase with higher CCN concentration (Fig. 8f), likely due to the enhanced latent heat release
 569 following the elevated condensational rate.

570 6. Conclusion and Discussion

571 The single-column versions of NCAR CAM5 and CAM6 are employed to simulate marine
 572 boundary-layer cloud and aerosol properties over the eastern North Atlantic during the ACE-ENA
 573 field campaign and to assess the uncertainty in cloud microphysical parameterizations. 3-hourly
 574 large-scale forcing data are derived from the systematic measurements of atmospheric states
 575 during the 8-month IOP. SCAM6 well reproduces the temperature field but overestimates specific
 576 and relative humidity by about 10%, especially for those near-cloud grid points. Our moisture
 577 adjustment simulation suggests that moisture variables in the large-scale forcing exert larger
 578 impacts on simulated cloud structures than cloud microphysics. It further implies ~~that~~ cloud
 579 microphysical properties are strongly regulated by the parameterizations, and less sensitive to the
 580 external forcing. Cloud frequency and transition between different types show good agreement
 581 between SCM and observation. Cloud ~~simulations~~ are generally improved from SCAM5 to
 582 SCAM6, in terms of droplet effective radius, cloud top height, and cloud thickness. However, there
 583 are some common issues with warm precipitation in those two models, ~~concerning~~ too small
 584 rainwater content and too frequent surface light precipitation.

585 To probe the possible contributions from the warm cloud parameterization to those drizzle
 586 biases, we implement the recalibrated autoconversion and accretion processes in the KK scheme
 587 ~~for both SCAM5 and SCAM6. The updated parameterizations~~ explicitly consider vertical
 588 variations of droplet size. ~~The new~~ scheme tends to improve CLWC and r_c in SCAM5 as well as
 589 $r_{m,r}$, but does not significantly alleviate the drizzle problem. The improvement is absent in

Deleted: very

Deleted: property

Deleted: including

Deleted: of

Deleted: that

Deleted: This updated

596 SCAM6, likely because sub-grid variations of cloud properties have been introduced in CAM6
597 cloud microphysics (especially for the autoconversion parameterization), suppressing the KK
598 scheme sensitivity to other factors. Further study is warranted to test whether the same warm rain
599 precipitation sensitivity holds for different cases using ~~SCAM5/6~~.

600 Aerosol simulations in SCAM6 are evaluated against the aircraft measurements during the
601 ACE-ENA. Significant Aitken-mode aerosol contribution to the CCN budget over ENA is
602 identified in both models and observations. SCAM6 agrees with observations on the magnitude of
603 concentration of accumulation-mode aerosol, CCN, and cloud droplets during the summer, while
604 N_{CCN} is significantly biased high from the surface to 2000 m in altitude during the winter. Aerosol
605 budget analyses show that in SCAM6, long-range transport provides too many Aitken-mode
606 sulfates that entrain into the MBL and can grow to CCN-size particles consequently. We further
607 quantify aerosol indirect effects by perturbing accumulation-mode aerosol concentrations in the
608 model. SCAM6 predicted cloud water and droplet size susceptibilities line up with the classic CCN
609 effects, i.e., reduced droplet size but enhanced liquid water content under the high CCN scenario.
610 The magnitudes of the cloud water and droplet size susceptibilities are also close to the LES
611 simulations conducted for the selected cases during the ACE-ENA.

612 The present study provides new insight of model biases in aerosol and warm cloud
613 simulations in the NCAR CAM models. Different from the previous evaluations of a full model
614 run with potential large biases propagated from modeled large-scale conditions, the model biases
615 discussed here, especially the drizzle property issue, should be adequately addressed in the future
616 development of CAM. The existing progress of predicted cloud properties and aerosol effects is
617 clearly demonstrated under the single-column framework in this study. More comprehensive
618 aerosol measurements, including Aitken- and coarse- mode aerosol properties, are needed in the
619 future field campaign to better understand the aerosol budget and aerosol-cloud interactions.

620

621 **Code availability**

622 The code of CESM model used in this study is available at
623 https://www.cesm.ucar.edu/models/cesm2/release_download.html.

624

625 **Data availability**

626 All the CESM model simulation input and output used for this research can be downloaded from

Deleted: SCM5

628 the website at <http://web.gps.caltech.edu/~yzw/share/Wang-2023-SCM>. The aircraft and ground-
629 based measurements used in this study were obtained from the Atmospheric Radiation
630 Measurement (ARM) Program sponsored by the U.S. Department of Energy (DOE) Office of
631 Energy Research, Office of Health and Environmental Research, and Environmental Sciences
632 Division. The [measurement](#) data can be downloaded from <http://www.archive.arm.gov/>.
633

634 **Competing interests**

635 Yuan Wang is a member of the editorial board of Atmospheric Chemistry and Physics.
636

637 **Acknowledgement**

638 This study was primarily supported by the collaborative NSF grant (Award No. AGS-2031751,
639 2031750). We thank the instrument mentors of the instruments and the individuals collecting
640 measurements during the ACE-ENA field campaign. We also acknowledge high-performance
641 computing support from NCAR Cheyenne. All requests for materials in this paper should be
642 addressed to Yuan Wang (yzwang@stanford.edu).

Deleted: yuanwang@purdue.edu

644 **References**

- 645 Bogenschutz, P. A., Gettelman, A., Morrison, H., Larson, V. E., Craig, C., and Schanen, D. P.:
646 Higher-Order Turbulence Closure and Its Impact on Climate Simulations in the Community
647 Atmosphere Model, *J. Climate*, 26, 9655-9676, 10.1175/JCLI-D-13-00075.1, 2013.
- 648 Copernicus Climate Change Service (C3S): ERA5: Fifth generation of ECMWF atmospheric
649 reanalyses of the global climate. Copernicus Climate Change Service Climate Data Store
650 (CDS), available at <https://cds.climate.copernicus.eu/cdsapp> (last access:), 2017.
- 651 Dong, X., Wu, P., Wang, Y., Xi, B., and Huang, Y.: New Observational Constraints on Warm
652 Rain Processes and Their Climate Implications, *Geophys. Res. Lett.*, 48, e2020GL091836,
653 <https://doi.org/10.1029/2020GL091836>, 2021.
- 654 Dong, X., Zheng, X., Xi, B., and Xie, S.: A climatology of mid-latitude maritime cloud fraction
655 and radiative effect derived from the ARM ENA ground-based observations, *J. Climate*, 1-
656 31, 10.1175/JCLI-D-22-0290.1, 2022.
- 657 Gettelman, A. and Morrison, H.: Advanced Two-Moment Bulk Microphysics for Global Models.
658 Part I: Off-Line Tests and Comparison with Other Schemes, *J. Climate*, 28, 1268-1287,
659 <https://doi.org/10.1175/JCLI-D-14-00102.1>, 2015a.
- 660 Gettelman, A., H. Morrison, S. Santos, P. Bogenschutz, and P. M. Caldwell: Advanced Two-
661 Moment Bulk Microphysics for Global Models. Part II: Global Model Solutions and Aerosol-
662 Cloud Interactions. *J. Climate*, 28, 1288-1307, <https://doi.org/10.1175/JCLI-D-14-00103.1>,
663 2015b.
- 664 Gettelman, A., Truesdale, J. E., Baumeister, J. T., Caldwell, P. M., Neale, R. B., Bogenschutz, P.
665 A., and Simpson, I. R.: The Single Column Atmosphere Model Version 6 (SCAM6): Not a
666 Scam but a Tool for Model Evaluation and Development, *Journal of Advances in Modeling*
667 *Earth Systems*, 11, 1381-1401, <https://doi.org/10.1029/2018MS001578>, 2019.
- 668 Golaz, J. C., Larson, V. E., and Cotton, W. R.: A PDF-based model for boundary layer clouds.
669 Part I: Method and model description, *J. Atmos. Sci.*, 59, 3540-3551, 2002.
- 670 Goldberger, L.: Passive cavity aerosol spectrometer probe aboard aircraft (PCASP-AIR) with
671 signal processing package 200 instrument handbook, DOE/SC-ARM-TR-241, Available from:
672 https://www.arm.gov/publications/tech_reports/handbooks/doe-sc-arm-tr-241.pdf, 2020.
- 673 Jensen, M. P., Ghate, V. P., Wang, D., Apoznanski, D. K., Bartholomew, M. J., Giangrande, S. E.,
674 Johnson, K. L., and Thieman, M. M.: Contrasting characteristics of open- and closed-cellular

675 stratocumulus cloud in the eastern North Atlantic, Atmos. Chem. Phys., 21, 14557-14571,
676 10.5194/acp-21-14557-2021, 2021.

677 Kay, J. E., and Coauthors: Exposing Global Cloud Biases in the Community Atmosphere Model
678 (CAM) Using Satellite Observations and Their Corresponding Instrument Simulators. J.
679 Climate, 25, 5190–5207, <https://doi.org/10.1175/JCLI-D-11-00469.1>, 2012.

680 Kay, J. E., Bourdages, L., Miller, N. B., Morrison, A., Yettella, V., Chepfer, H., and Eaton, B.:
681 Evaluating and improving cloud phase in the Community Atmosphere Model version 5 using
682 spaceborne lidar observations, J. Geophys. Res.-Atmos., 121, 4162-4176,
683 <https://doi.org/10.1002/2015JD024699>, 2016.

684 Khairoutdinov, M. & Kogan, Y. A New Cloud Physics Parameterization in a Large-Eddy
685 Simulation Model of Marine Stratocumulus. Mon. Weather Rev. 128, 229–243, 2000.

686 Lebsock, M., Morrison, H., and Gettelman, A., Microphysical implications of cloud-precipitation
687 covariance derived from satellite remote sensing, J. Geophys. Res. Atmos., 118, 6521– 6533,
688 [doi:10.1002/jgrd.50347](https://doi.org/10.1002/jgrd.50347), 2013.

689 Li, F. and Lawrence, D. M.: Role of Fire in the Global Land Water Budget during the Twentieth
690 Century due to Changing Ecosystems, J. Climate, 30, 1893-1908, [https://doi.org/10.1175/JCLI-](https://doi.org/10.1175/JCLI-D-16-0460.1)
691 [D-16-0460.1](https://doi.org/10.1175/JCLI-D-16-0460.1), 2017.

692 Liu, X. and Penner, J.E.: Ice Nuclei Parameterization for Global Model. Meteorologische
693 Zeitschrift, 14, 499-514, <https://doi.org/10.1127/0941-2948/2005/0059>, 2005.

694 Liu, X., Penner, J. E., Ghan, S. J., and Wang, M.: Inclusion of Ice Microphysics in the NCAR
695 Community Atmospheric Model Version 3 (CAM3), J. Climate, 20, 4526-4547,
696 <https://doi.org/10.1175/JCLI4264.1>, 2007.

697 Liu, X., Ma, P. L., Wang, H., Tilmes, S., Singh, B., Easter, R. C., Ghan, S. J., and Rasch, P. J.:
698 Description and evaluation of a new four-mode version of the Modal Aerosol Module (MAM4)
699 within version 5.3 of the Community Atmosphere Model, Geosci. Model Dev., 9, 505-522,
700 10.5194/gmd-9-505-2016, 2016.

701 Malavelle, F. F., Haywood, J. M., Jones, A., Gettelman, A., Clarisse, L., Bauduin, S., Allan, R. P.,
702 Karset, I. H. H., Kristjánsson, J. E., Oreopoulos, L., Cho, N., Lee, D., Bellouin, N., Boucher,
703 O., Grosvenor, D. P., Carslaw, K. S., Dhomse, S., Mann, G. W., Schmidt, A., Coe, H., Hartley,
704 M. E., Dalvi, M., Hill, A. A., Johnson, B. T., Johnson, C. E., Knight, J. R., O'Connor, F. M.,
705 Partridge, D. G., Stier, P., Myhre, G., Platnick, S., Stephens, G. L., Takahashi, H., and

Formatted: Left

Deleted: ↵

707 Thordarson, T.: Strong constraints on aerosol–cloud interactions from volcanic eruptions,
 708 Nature, 546, 485-491, 10.1038/nature22974, 2017.

709 Sherwood, S. C., Webb, M. J., Annan, J. D., Armour, K. C., Forster, P. M., Hargreaves, J. C.,
 710 Hegerl, G., Klein, S. A., Marvel, K. D., Rohling, E. J., Watanabe, M., Andrews, T., Braconnot,
 711 P., Bretherton, C. S., Foster, G. L., Hausfather, Z., von der Heydt, A. S., Knutti, R., Mauritsen,
 712 T., Norris, J. R., Proistosescu, C., Rugenstein, M., Schmidt, G. A., Tokarska, K. B., and Zelinka,
 713 M. D.: An Assessment of Earth's Climate Sensitivity Using Multiple Lines of Evidence,
 714 Reviews of Geophysics, 58, e2019RG000678, <https://doi.org/10.1029/2019RG000678>, 2020.

715 Tang, S., C. Tao, S. Xie and M. Zhang: Description of the ARM Large-Scale Forcing Data from
 716 the Constrained Variational Analysis (VARANAL) Version 2, DOE ARM Climate Research
 717 Facility, Technical Report DOE/SC-ARM-TR-222. Available at:
 718 https://www.arm.gov/publications/tech_reports/doe-sc-arm-tr-222.pdf, 2019

719 Uin, J., and F. Mei: Cloud condensation nuclei particle counter instrument handbook – airborne
 720 version, DOE/SC-ARM-TR-225, Available from:
 721 https://www.arm.gov/publications/tech_reports/handbooks/doe-sc-arm-tr-225.pdf, 2019

722 Wang, J., Wood, R., Jensen, M. P., Chiu, J. C., Liu, Y., Lamer, K., Desai, N., Giangrande, S. E.,
 723 Knopf, D. A., Kollias, P., Laskin, A., Liu, X., Lu, C., Mechem, D., Mei, F., Starzec, M.,
 724 Tomlinson, J., Wang, Y., Yum, S. S., Zheng, G., Aiken, A. C., Azevedo, E. B., Blanchard, Y.,
 725 China, S., Dong, X., Gallo, F., Gao, S., Ghate, V. P., Glienke, S., Goldberger, L., Hardin, J. C.,
 726 Kuang, C., Luke, E. P., Matthews, A. A., Miller, M. A., Moffet, R., Pekour, M., Schmid, B.,
 727 Sedlacek, A. J., Shaw, R. A., Shilling, J. E., Sullivan, A., Suski, K., Veghte, D. P., Weber, R.,
 728 Wyant, M., Yeom, J., Zawadowicz, M., and Zhang, Z.: Aerosol and Cloud Experiments in the
 729 Eastern North Atlantic (ACE-ENA), B. Am. Meteorol. Soc., 1-51, 10.1175/BAMS-D-19-
 730 0220.1, 2021.

731 Wang, Y., Fan, J., Zhang, R., Leung, L. R. and Franklin, C.: Improving bulk microphysics
 732 parameterizations in simulations of aerosol effects, J. Geophys. Res. Atmos.,
 733 doi:10.1002/jgrd.50432, 2013.

734 Wang, Y., Wang, M., Zhang, R., Ghan, S. J., Lin, Y., Hu, J., Pan, B., Levy, M., Jiang, J. H. and
 735 Molina, M. J.: Assessing the effects of anthropogenic aerosols on Pacific storm track using a
 736 multiscale global climate model, Proc. Natl. Acad. Sci. U. S. A.,
 737 doi:10.1073/pnas.1403364111, 2014.

738 Wang, Y., Jiang, J. H., and Su, H.: Atmospheric responses to the redistribution of anthropogenic
739 aerosols, *J. Geophys. Res.-Atmos.*, 120, 9625-9641, <https://doi.org/10.1002/2015JD023665>,
740 2015.

741 Wang, Y., ~~P.-L. Ma~~, J. Jiang, ~~H. Su~~ and ~~P. Rasch~~, Towards Reconciling the Influence of
742 Atmospheric Aerosols and Greenhouse Gases on Light Precipitation Changes in Eastern
743 China, *J. Geophys. Res. Atmos.* 121(10), 5878–5887, 2016.

744 Wang, Y., P. Ma, J. Peng, R. Zhang, J.H. Jiang, R. Easter and Y. Yung, Constraining Aging
745 Processes of Black Carbon in the Community Atmosphere Model Using Environmental
746 Chamber Measurements, *J. Adv. Model. Earth Syst.* 10(10), 2514-2526, 2018.

747 Wang, Y., Zheng, X., Dong, X., Xi, B., Wu, P., Logan, T., and Yung, Y. L.: Impacts of long-range
748 transport of aerosols on marine-boundary-layer clouds in the eastern North Atlantic, *Atmos.*
749 *Chem. Phys.*, 20, 14741-14755, 10.5194/acp-20-14741-2020, 2020.

750 Wang, Y., Zheng, G., Jensen, M. P., Knopf, D. A., Laskin, A., Matthews, A. A., Mechem, D., Mei,
751 F., Moffet, R., Sedlacek, A. J., Shilling, J. E., Springston, S., Sullivan, A., Tomlinson, J.,
752 Veghte, D., Weber, R., Wood, R., Zawadowicz, M. A., and Wang, J.: Vertical profiles of
753 trace gas and aerosol properties over the eastern North Atlantic: variations with season and
754 synoptic condition, *Atmos. Chem. Phys.*, 21, 11079-11098, 10.5194/acp-21-11079-2021,
755 2021.

756 Wu, P., Dong, X., Xi, B., Tian, J., and Ward, D. M.: Profiles of MBL Cloud and Drizzle
757 Microphysical Properties Retrieved From Ground-Based Observations and Validated by
758 Aircraft In Situ Measurements Over the Azores, *J. Geophys. Res.-Atmos.*, 125, e2019JD032205,
759 <https://doi.org/10.1029/2019JD032205>, 2020.

760 Xie, S. C., Cederwall, R. T., and Zhang, M. H.: Developing long-term single-column model/cloud
761 system-resolving model forcing data using numerical weather prediction products constrained
762 by surface and top of the atmosphere observations, *Journal of Geophysical Research-*
763 *Atmospheres*, 109(D1), doi: 10.1029/2003jd004045, 2004

764 Yeager, S. G., Danabasoglu, G., Rosenbloom, N. A., Strand, W., Bates, S. C., Meehl, G. A.,
765 Karspeck, A. R., Lindsay, K., Long, M. C., Teng, H., and Lovenduski, N. S.: Predicting Near-
766 Term Changes in the Earth System: A Large Ensemble of Initialized Decadal Prediction
767 Simulations Using the Community Earth System Model, *B. Am. Meteorol. Soc.*, 99, 1867-1886,
768 <https://doi.org/10.1175/BAMS-D-17-0098.1>, 2018.

Deleted: Vogel

Deleted: M., Lin, Y., Pan, B., Hu, J., Liu, Y., Dong, X.,

Deleted: J.

Deleted: ., Yung, Y. L.

Deleted: Zhang, R.: Aerosol microphysical

Deleted: radiative effects

Deleted: continental cloud ensembles, Adv.

Deleted: Sci., doi:

Deleted: .1007/s00376-017-7091-5, 2018

778 Zawadowicz, M. A., Suski, K., Liu, J., Pekour, M., Fast, J., Mei, F., Sedlacek, A. J., Springston,
 779 S., Wang, Y., Zaveri, R. A., Wood, R., Wang, J., and Shilling, J. E.: Aircraft measurements of
 780 aerosol and trace gas chemistry in the eastern North Atlantic, *Atmos. Chem. Phys.*, 21, 7983-
 781 8002, 10.5194/acp-21-7983-2021, 2021.
 782 Zhang, G. J. and McFarlane, N. A.: Sensitivity of climate simulations to the parameterization of
 783 cumulus convection in the Canadian climate centre general circulation model, *Atmosphere-
 784 Ocean*, 33, 407-446, 10.1080/07055900.1995.9649539, 1995.
 785 Zhang, Z., Song, H., Ma, P.-L., Larson, V. E., Wang, M., Dong, X., and Wang, J.: Subgrid
 786 variations of the cloud water and droplet number concentration over the tropical ocean: satellite
 787 observations and implications for warm rain simulations in climate models, *Atmos. Chem.*
 788 *Phys.*, 19, 1077–1096, <https://doi.org/10.5194/acp-19-1077-2019>, 2019.
 789 Zhao, L., Wang, Y., Zhao, C., Dong, X., and Yung, Y. L.: Compensating Errors in Cloud Radiative
 790 and Physical Properties over the Southern Ocean in the CMIP6 Climate Models, *Adv. Atmos.*
 791 *Sci.*, 39, 2156-2171, 10.1007/s00376-022-2036-z, 2022.
 792 Zhao, X., Liu, X., Phillips, V. T. J., and Patade, S.: Impacts of secondary ice production on Arctic
 793 mixed-phase clouds based on ARM observations and CAM6 single-column model simulations,
 794 *Atmos. Chem. Phys.*, 21, 5685-5703, 10.5194/acp-21-5685-2021, 2021.
 795 Zheng, X., Xi, B., Dong, X., Wu, P., Logan, T., and Wang, Y.: Environmental effects on aerosol–
 796 cloud interaction in non-precipitating marine boundary layer (MBL) clouds over the eastern
 797 North Atlantic, *Atmos. Chem. Phys.*, 22, 335-354, 10.5194/acp-22-335-2022, 2022a.
 798 Zheng, X., Dong, X., Ward, D. M., Xi, B., Wu, P., and Wang, Y.: Aerosol-Cloud-Precipitation
 799 Interactions in a Closed-cell and Non-homogenous MBL Stratocumulus Cloud, *Adv. Atmos.*
 800 *Sci.*, 39, 2107-2123, 10.1007/s00376-022-2013-6, 2022b.
 801

Table 1. Comparison of physical parameterizations relevant with warm cloud processes between CAM5 and CAM6.

<u>Model Physics</u>	<u>CAM5</u>	<u>CAM6</u>
<u>Cloud Microphysics</u>	<u>MG1 (Morrison and Gettelman, 2008) with KK scheme for warm rain processes.</u>	<u>MG2 with retuned autoconversion, explicit sub-grid variance of cloud, and prognostic rain and snow (Morrison and Gettelman, 2015)</u>
<u>Stratiform Macrophysics</u>	<u>The Park scheme (Park et al., 2014)</u>	<u>The Cloud Layers Unified By Binormals (CLUBB), a prognostic moist turbulence scheme that unifies the representation of boundary layer, shallow convection, and stratiform macrophysics (Golaz and Larson, 2002)</u>
<u>PBL and shallow convection scheme</u>	<u>The University of Washington scheme (Park and Bretherton, 2009)</u>	
<u>Aerosol</u>	<u>3-mode Modal Aerosol Module (MAM3, Ghan et al., 2011)</u>	<u>4-mode Modal Aerosol Module (MAM4) with a new “fresh-BC” mode (Liu et al., 2016)</u>

806 **Table 2.** Single-column numerical experiment design.
807

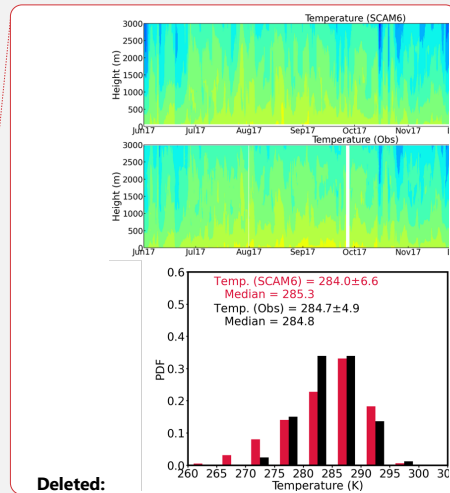
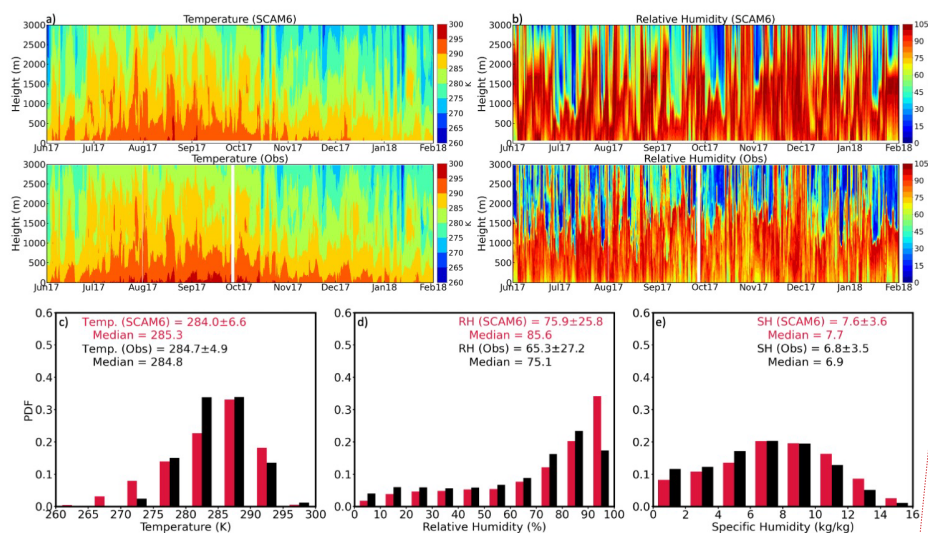
|

Model Physics	Experiment Name	Experiment Description
CAM6	Ctrl	Default model setup and forcing data
	D21	Using recalibrated warm rain parameterizations similar to Dong et al. (2021)
	pAero	Scale up aerosol number and mass concentrations in the accumulation mode by a factor of 2 in the initial condition
	ForcingQ_Adj	Adjust specific humidity state variable and related tendency terms by a factor of 0.85
CAM5	Ctrl	Default model setup and forcing data
	D21	Using recalibrated warm rain parameterizations based on Dong et al. (2021)

808

Deleted: based on

810 Figures



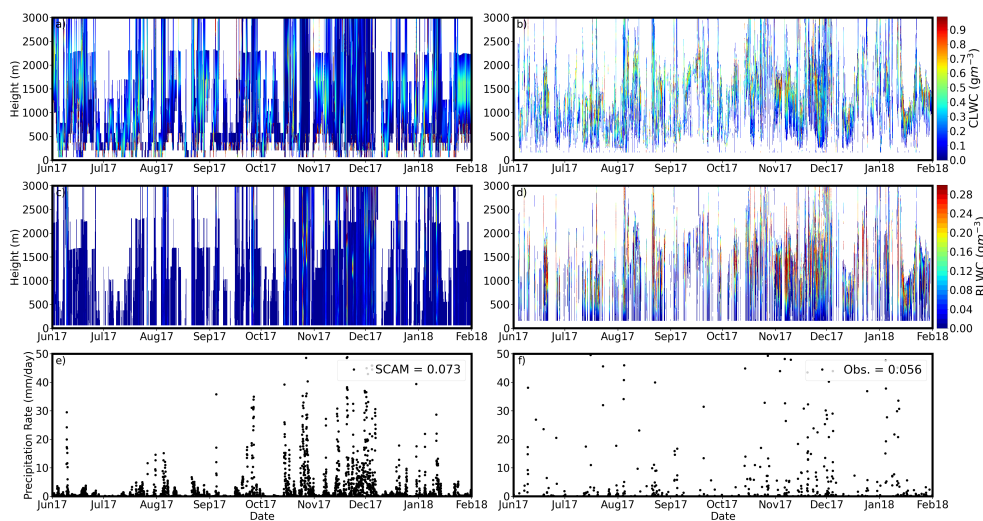


Figure 2. Time series of the cloud liquid water contents (CLWC, top panels), rain liquid water contents (RLWC, middle panels) and surface precipitation (bottom panels) from the SCAM6 simulations (left column) and the ARM-ENA retrievals and observations (right column).

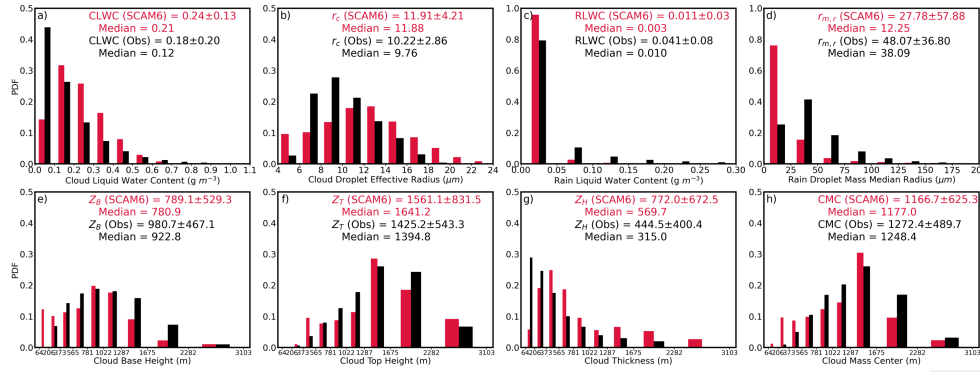


Figure 3. Probability distribution functions (PDFs), mean, standard deviation, and median values of cloud and rain microphysics, and cloud macrophysics simulated from SCAM6 (red) and observed/retrieved from ground-based remote sensors (black). (a) Cloud liquid water content, CLWC; (b) Cloud droplet effective radius, r_c ; (c) Rain liquid water content, RLWC; (d) Rain droplet mass median radius, $r_{m,r}$; (e) Cloud base height, Z_B ; (f) Cloud top height, Z_T ; (g) Cloud thickness, Z_H and (h) Cloud mass center.

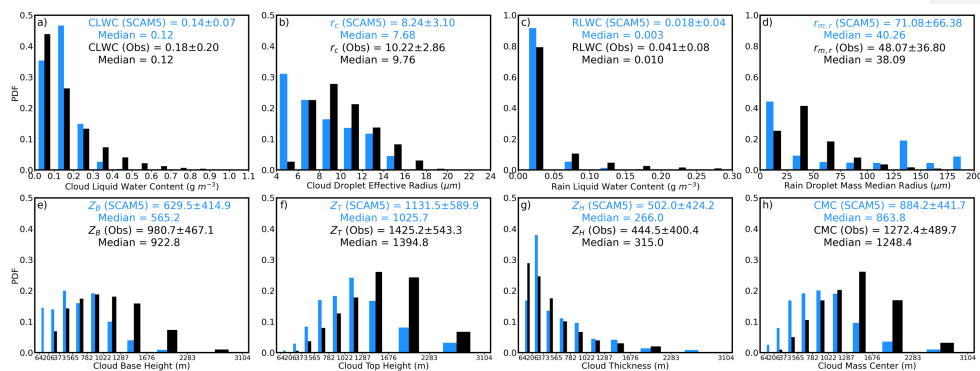


Figure 4. Same as Fig 3, except for SCAM5 (blue).

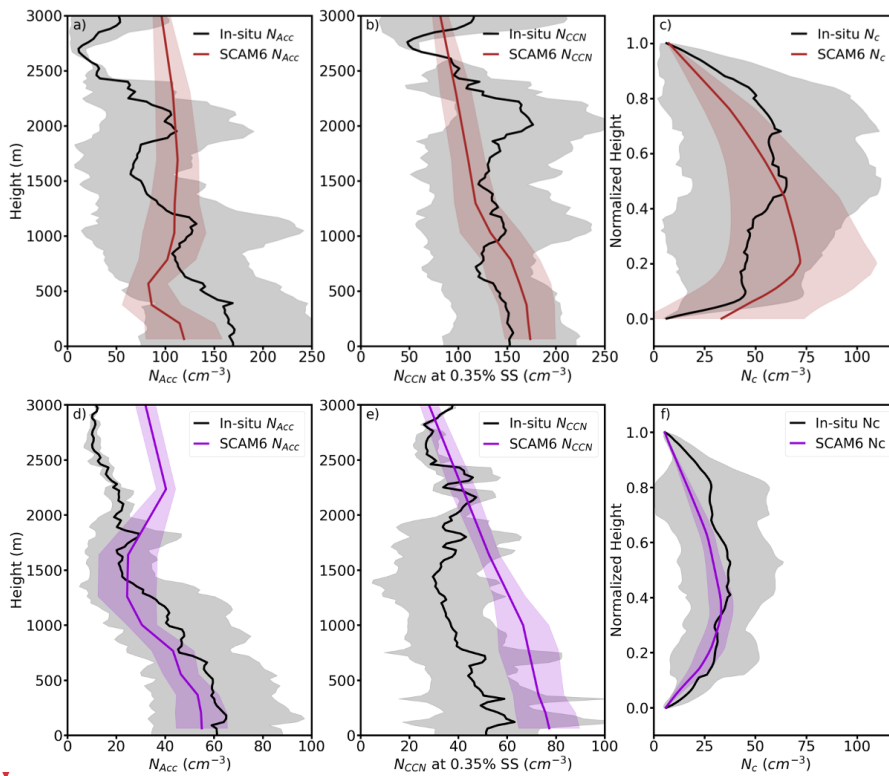


Figure 5. Vertical profiles of accumulation mode aerosol (N_{ACC}) (a, d); CCN concentration (N_{CCN}) at 0.35% supersaturation (b, e) during interstitial conditions, and Cloud droplet number concentration (N_c) at normalized height (c, f, 0 is cloud base, 1 is cloud top) for cloudy samples. For SCAM6 simulations (brown and purple) and aircraft in situ measurement (black), during the Summer (top panels) and Winter (bottom panels) ACE-ENA IOPs. The shaded areas denote the standard deviation at each level. The SCAM6 simulations are selected within each time duration of the aircraft cases. The reason of using normalized height for N_c is that the cloud layer thickness and vertical positions differ for each corresponding time stamp. We need to normalize the height within each cloud layer to ensure that the N_c vertical variation is representative.

Deleted: <object><object>

Deleted: N_c

Deleted: -

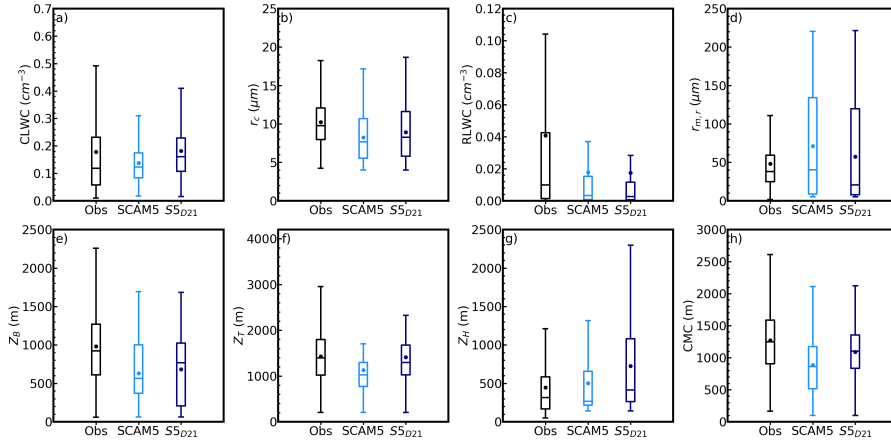


Figure 6. Comparisons of cloud and rain microphysics, and cloud macrophysics between observations (black), SCAM5 (blue) and SCAM5 with Dong2021 parameterization ($SCAM5_{D21}$, dark blue). (a) $CLWC$, (b) r_c , (c) $RLWC$, (d) $r_{m,d}$, (e) Z_B , (f) Z_T , (g) Z_H , and (h) Cloud mass center. Dots represent the mean values, and the bars from bottom to top represent 10%, 25%, 50%, 75%, and 90% values, respectively.

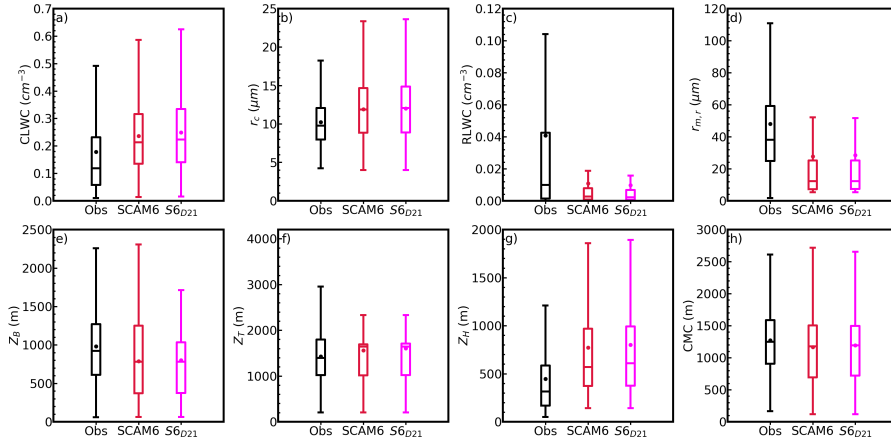


Figure 7. Same as Fig 6, except for SCAM6 (red), and SCAM6 with Dong2021 parameterization (SCAM6_{D21}, pink).

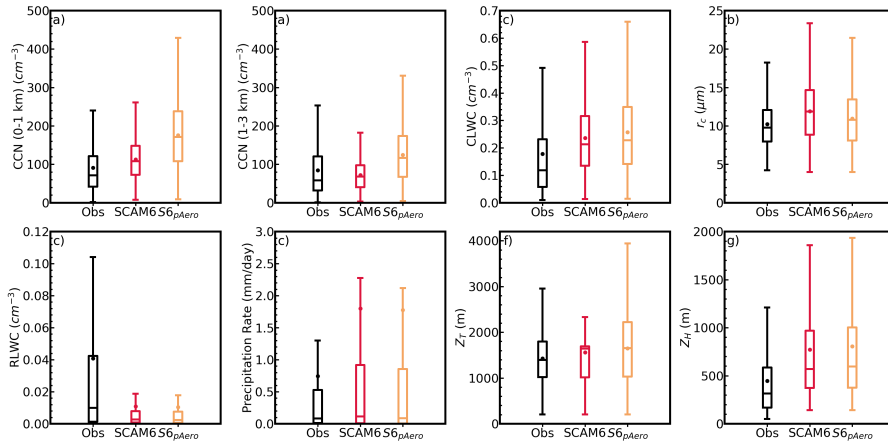


Figure 8. Aerosol and cloud properties simulated from control (red) and aerosol-perturbing experiments (pAero, orange) by SCAM6 and comparison to observations. The observed CCN at 0.35% SS are averaged from the selected aircraft measurements during the ACE-ENA.

Page 13: [1] Deleted Yuan Wang 5/31/23 1:15:00 PM

▼
Page 13: [2] Deleted Yuan Wang 5/31/23 1:15:00 PM

▼
Page 13: [3] Deleted Yuan Wang 5/31/23 1:15:00 PM

▼